*ADMET & DMPK 2(2) (2014) 126-142; doi: **10.5599/admet.2.2.28***

ADMET

Open Access : ISSN : 1848-7718

http://www.pub.iapchem.org/ojs/index.php/admet/index

Original scientific paper

Human Serum Albumin Binding of 2-[(Carboxymethyl)sulfanyl]-4-oxo-4-(4-*tert*-butylphenyl)butanoic Acid and its Mono-Me Ester

Ilija N. Cvijetić, Dušan D. Petrović,[1] Tatjana Ž. Verbić,[1,]* Ivan O. Juranić[2] and Branko J. Drakulić[2]

Innovation Center of the Faculty of Chemistry, University of Belgrade, Studentski Trg 16, 11000 Belgrade, Serbia
[1]Faculty of Chemistry, University of Belgrade, Studentski Trg 16, 11000 Belgrade, Serbia
[2]Department of Chemistry-IChTM, University of Belgrade, Njegoševa 12, 11000 Belgrade, Serbia

*Corresponding Author: E-mail: tatjanad@chem.bg.ac.rs ; Tel.: +381-11-3336-790; Fax: +381-11-2184-330

Received: December 21, 2013; Revised: April 22, 2014; Published: July 18, 2014

Abstract

*Interactions of 2-[(carboxymethyl)sulfanyl]-4-oxo-4-(4-*tert*-butylphenyl)butanoic acid (compound **1**) and its mono-Me ester (compound **2**) with the human serum albumin (HSA) have been studied by fluorescence spectroscopy. Comp. **1** exerts antiproliferative activity toward human tumor cells and significant selectivity (tumor vs. healthy cells)* in vitro*. Competitive binding study with warfarin and ibuprofen as binding site probes, revealed that one molecule of comp. **1** selectively binds to HSA Sudlow site I (warfarin site) with moderate binding constant ($K_b = (2.8 \pm 0.5) \times 10^4$ M^{-1} at 37 ± 1 °C), while comp. **2** binds to Sudlow site II ($K_b = (3.2 \pm 0.9) \times 10^4$ M^{-1} at 37 ± 1 °C). Fluorescence quenching at different temperatures was analyzed using classical Stern-Volmer equation, and a static quenching mechanism was proposed. Energy resonance transfer between HSA and comp. **1** was examined according to Förster's non-radiative energy transfer theory. Distance of about 10 Å between ligand and Trp214 (HSA) was obtained. Docking studies confirmed HSA Sudlow site I as a preferable comp. **1** binding site, and Sudlow site II as comp. **2** binding site. Molecular dynamics simulations proved the stability of comp. **1**/HSA complex.*

Keywords: Fluorescence spectroscopy; competitive binding; molecular dynamics; molecular docking

1. Introduction

2-[(Carboxymethyl)sulfanyl]-4-oxo-4-phenyl)butanoic acids (CSAB) exert antiproliferative activity toward human tumor cell lines in low micromolar to submicromolar concentrations and significant selectivity. Depending on substitution pattern on the aroyl ring, it was shown that some congeners are significantly less toxic toward healthy human cells, comparing to tumor cells, *in vitro* [1]. Low compounds' toxicity tested on animal model (*in vivo*) was also proved [2]. Within the frame of physico-chemical profiling of CSAB, we report human serum albumin binding of the derivative bearing 4-*tert*-Bu-group on aroyl ring (**1**) and its mono-Me ester (**2**), Figure 1.

Human serum albumin (HSA) is the most abundant protein in blood plasma and tissue fluids (concentration in serum approximately 0.6 mM) and plays an important role in osmotic pressure and pH regulation, transport of endogenous (fatty acids, hormones, bile acids, amino acids, etc.) and exogenous

compounds (drug molecules and nutrients). HSA performs other functions such as sequestering oxygen free radicals and inactivating various toxic lipophilic metabolites [3]. It is a monomeric polypeptide that folds into three structurally distinct and evolution-related helical domains (I-III). Each domain comprises two subdomains (A and B), possessing common structural motifs, connected by a random coil (Figure 2). Two out of six binding sites have been identified as primary sites for the binding of drugs and drug-like compounds [4,5]. Sudlow site I is located in subdomain IIA. Low stereoselectivity of this site toward small organic molecules (SOM) might be ascribed to its flexibility. Ligands that strongly bind to site I are generally supposed to be dicarboxylic acids and/or bulky heterocyclic molecules with a negative charge localized in the middle of the molecule (warfarin, azapropazone, phenylbutazone, etc.). Sudlow site II is located in subdomain IIIA, and is smaller, but topologically similar to site I. Site II appears to be less flexible, since ligand binding to this site often shows stereoselectivity, and binding is strongly affected by small structural modifications of the ligand. Site II (also called the indole-benzodiazepine site) preferably accommodates aromatic carboxylic acids, with a negative charge located distant from the hydrophobic region of the molecule. It is specific for ibuprofen, 1-anilino-8-naphthalene sulfonic acid (ANS), diazepam, dansylsarcosine, etc. However, these structural features are not strict prerequisites for site I and site II binding, since numerous ligands are known to bind to both drug binding sites, though with different affinities [6].

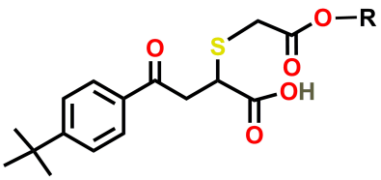

Figure 1. *Structure of 2-[(carboxymethyl)sulfanyl]-4-oxo-4-(4-*tert*-butylphenyl)butanoic acid (4-*tert*-Bu-CSAB, R = H, comp.* ***1****) and its Me-ester (R = Me, comp.* ***2****).*

The SOM in blood circulation can exist as free (unbound) form, or bound to plasma proteins (PP). Weak PP binding leads to a short lifetime or poor tissue distribution of SOM, whereas strong binding decreases the concentrations of free SOM in plasma. Consequently, investigations of the lead compounds' affinity to serum albumin, and the corresponding interaction mechanisms, along with other important ADME/Tox properties (CYP450 transformation, hERG blockade, volume of distribution, etc.), may provide useful information about their pharmacokinetics [6,7].

Binding of SOM to proteins is studied by different instrumental techniques [8-12]. Fluorescence measurements are often used to study SOM binding to proteins because information on binding mechanism, binding mode, binding constants, binding sites, intermolecular distances, etc., can be easily obtained. Fluorescence of albumins mostly originates from two types of fluorophores: tryptophanyl and tyrosyl [13]. Tryptophan, tyrosine, and phenylalanine are three fluorophores in HSA (and in the majority of other proteins), but the fluorescence of HSA almost exclusively originates from tryptophan 214 (Trp214) alone. Phenylalanine has a very low quantum yield and the fluorescence of tyrosine is almost entirely quenched if it is near to an amino group, a carboxyl group, or a tryptophan. Upon binding of SOM to HSA, changes of intrinsic fluorescence intensity of HSA become induced by the microenvironment of Trp214 [14].

Computational methods, such as molecular dynamics (MD) simulations and molecular docking, are very useful tools for studying the protein-ligand interactions. MD is often used for simulations of protein conformational changes upon binding to ligand. If the position, or the orientation, of the ligand in protein

binding site is unknown, docking simulations are the most often used *in silico* method for obtaininig the input for MD simulation.

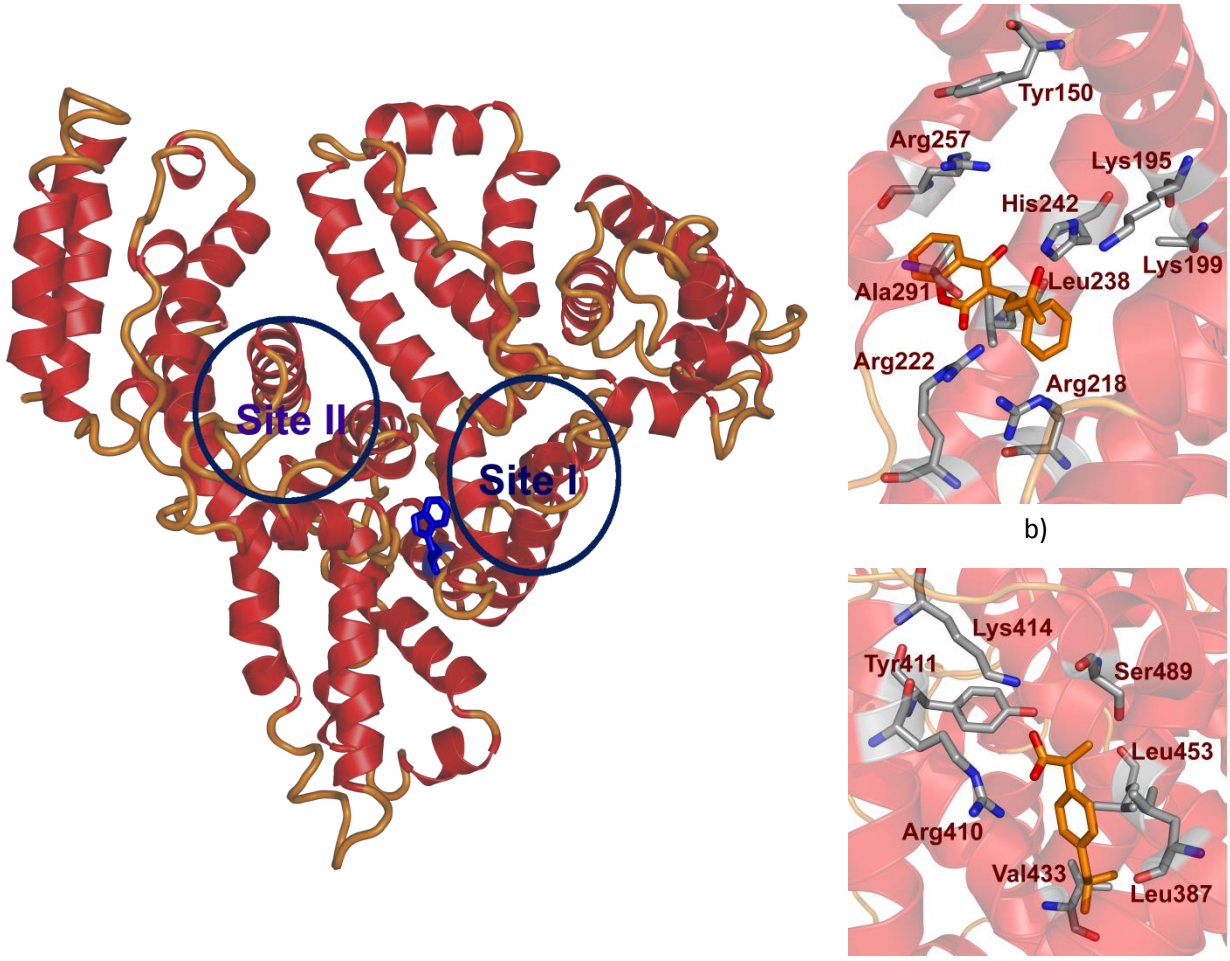

***Figure 2**. a) Structure of HSA (PDB ID 1BJ5) and the location of major binding sites, Trp214 is depicted in stick representation. b) Sudlow site I, with bound warfarin, is depicted from the PDB entry 2BXD. c) Sudlow site II, with bound ibuprofen is depicted from the PDB entry 2BGX.*

In the present work, we used combination of experimental and computational techniques in order to find the location and to estimate the strength of compounds **1** and **2** binding to HSA. The number of binding sites per HSA molecule has also been determined. The fluorescence quenching mechanism was proposed according to the fluorescence measurements at different temperatures. Competitive binding experiments, using specific binding site probes (warfarin and ibuprofen), revealed the specific sites of comp. **1** and comp. **2** binding to HSA. Along with this, the possibility of resonance energy transfer between HSA as a donor, and comp. **1** as an acceptor of electron excitation were examined according to the Förster's resonance energy transfer (FRET) theory [15,16]. Binding of both compounds to HSA was also studied by molecular docking, and the stability of comp. **1**/HSA complex evaluated by molecular dynamics simulations.

2. Experimental

2.1. Reagents and Apparatus

Human serum albumin (HSA) was kindly provided by Blood Transfusion Institute of Serbia and purified according to standard procedure [17]. The concentration of purified HSA was determined using Bradford method [18].

Phosphate buffered saline (PBS) was used to maintain the physiological pH value (pH 7.34). Potassium dihydrogen phosphate, disodium hydrogen phosphate, sodium chloride, and potassium chloride used for PBS preparation, as well as warfarin and ibuprofen, were purchased from Sigma-Aldrich. All solutions were prepared with Millipore water.

Fluorescence spectra were recorded on Horiba Jobin Yvon Fluoromax-4 spectrometer, equipped with Peltier element and magnetic stirrer for cuvette, using quartz cell with 1 cm path length and 4 mL volume. An excitation wavelength was 280 nm, with 5 nm slits; emission spectra were recorded in 300-450 nm wavelength range, with 5 nm slits, and 0.1 s integration time. Background PBS signal was subtracted from the each spectrum.

UV/Vis spectra were recorded on GBC Cintra 6 spectrophotometer (GBC Dandenong, Australia) using quartz cell with 1 cm path length and 4 mL volume. All spectra were recorded against the corresponding blank (1× PBS) in the 220-450 nm wavelength range, with 500 nm/min scan speed.

2.2. Methods

2.2.1. Spectroscopy

Stock solutions of HSA ($c = 1.08 \times 10^{-3}$ M), comp. **1** ($c_1 = 1.12 \times 10^{-3}$ M), comp. **2** ($c_2 = 1.62 \times 10^{-3}$ M) warfarin ($c = 4.38 \times 10^{-4}$ M), and ibuprofen ($c = 4.61 \times 10^{-4}$ M) were prepared in 1× PBS, pH 7.34, and kept in refrigerator. For comp. **1** and **2** /HSA interaction studies, HSA solution was freshly prepared from the stock, by dilution with a buffer (HSA concentration was kept constant, $c = 1 \times 10^{-6}$ M), and titrated with comp. **1** or **2** stock solution to avoid large sample dilution. Upon addition of each aliquot, system was stirred and left to equilibrate for 15 min, before UV/Vis absorption and fluorescence emission spectra recording. For competitive binding experiments, solution containing HSA ($c = 1 \times 10^{-6}$ M) and binding site probe (warfarin or ibuprofen, $c = 1 \times 10^{-6}$ M) was stirred and left to equilibrate for 1 h. Afterwards, titration with compounds **1** or **2** was performed as described above. All experiments were performed in triplicates and values reported as mean values.

In order to remove the inner filter effect originating from HSA and studied compounds, the absorbancies were measured at the excitation (280 nm) and emission (340 nm) wavelengths, and fluorescence intensities corrected according to Lakowicz equation (1):

$$F_{corr} = F_{obs} 10^{\frac{A_{ex} + A_{em}}{2}} \quad (1)$$

where F_{corr} and F_{obs} are corrected and observed fluorescence intensities, and A_{ex} and A_{em} are absorbancies at the excitation and emission wavelengths, respectively [19]. Corrected fluorescence intensities were used for further calculations.

^{1}H and ^{13}C NMR spectra were recorded in $CDCl_3$ on a Bruker Avance 500/125 MHz instrument. ESI-MS spectra were recorded on Agilent Technologies 6210-1210 TOF-LC-ESI-HR/MS instrument in positive mode.

*2.2.2. S*ynthesis

The preparation and characterization of the comp. **1** were described earlier [1]. Compound **2** was obtained by mixing 180 mg (7.75×10^{-4} mol) of (*E*)-4-(4-*tert*-Bu-phenyl)-4-oxobut-2-enoic acid and 1.3 mol equivalents (107 mg) of thioglycolic acid Me-ester during 20 h in 15 mL of MeOH. The volume of the solvent was then reduced to approx. 1/8 of the initial, the product precipitated with hexanes/Et_2O (approx. 4 : 1; 8 mL), and collected by filtration. Crude product was rinsed with small amount of Et_2O on the funnel, then dried on air. 180 mg of the isolated product was obtained (69 % of the theoretical yield). Product is characterized by ^{1}H and ^{13}C NMR and LC/HR-MS, confirming > 98% purity.

(*R*, *S*)-4-(4-*tert*-Bu-phenyl)-2-[(2-methoxy-2-oxoethyl)sulfanyl]-4-oxobutanoic acid, $C_{17}H_{22}O_5S$: ^{1}H NMR (500 MHz, $CDCl_3$) δ 9.04 (br. s., 1H), 7.88 (d, J = 8.59 Hz, 2H), 7.47 (d, J = 8.59 Hz, 2H), 4.01-4.04 (dd, $J_{1,2}$ = 4.74, $J_{1,3}$ = 9.82 Hz, 1H), 3.75 (s, 3H), 3.63-3.69 (dd, $J_{1,2}$ = 9.82, $J_{1,3}$ = 17.89 Hz, 1H), 3.57 (q, $J_{1,2}$ = 15.96, $J_{1,3}$ = 67 Hz, 2H), 3.35-3.40 (dd, $J_{1,2}$ = 4.74, $J_{1,3}$ = 17.89 Hz, 1H), 1.33 (s, 9H); ^{13}C NMR (125 MHz, $CDCl_3$) δ 196.0, 176.8, 170.7, 157.5, 133.2, 128.1, 125.6, 52.7, 41.4, 40.3, 35.1, 33.7, 31.0; LC/ESI-HR-MS: 339.12551 (M+1 calculated), 339.12607 (M+1, measured).

2.2.3. Molecular modeling

3D Structure of comp. **1** and **2** were obtained in OMEGA 2.5.1.4 [20,21] as the global energy minima using MMFF94s force field [22]. After deprotonation of carboxyl groups, structures were further minimized in MOPAC2012 program [23,24] by semiempirical molecular orbital PM6 method [25]. Structure of the HSA was prepared in VegaZZ 3.0.1 [26].

Docking of both compounds was done by AutoDock Vina 1.1 [27]. For docking studies, H atoms were added to the HSA structure (PDB ID 1BJ5 [28]), the system was neutralized (18 Na^+ ions added) and embedded in explicit solvent (water) sphere encompassing 35 Å from the protein boundary. Molecules of myristic acid, cocrystallized with the protein, were retained. Similar procedure was used to prepare comp. **1**/HSA complex for MD. CHARMm22 force field and Gasteiger charges were used for MD simulations. Solvated protein and protein/comp. **1** complex were minimized at 300 K, during 30000 steps (30 ps). The last frame from the minimization was used for heating of the system to 300 K (10000 steps, 10 ps). The system prepared in this way was submitted to 3 ns of unconstrained MD simulation. Structures of compounds **1** and **2** were docked in the whole structure of HSA, using grid resolution of 1 Å (default in Vina). Exhaustiveness was set to 100. Compounds **1** and **2** were treated as flexible, while protein side-chains were treated as rigid. Best docking solutions of compounds **1** and **2** were optimized and rescored by Fred Rescore, the part of OEDocking suite [29-31]. All MD simulations were performed in NAMD 2.9 [32] in Linux environment, on multi-node cluster [33] equipped with the dual Intel Xeon X5560 @ 2.8 GHz processors.

Computations in GRID [34] were performed with the carboxylate anion (COO^-) probe in the box encompassing the whole protein, or with the water probe (OH2) in the boxes encompassing Sudlow sites I and II, separately, using grid resolution of 0.3 Å. The movement of protein side-chains during calculations was allowed in calculations with COO^- probe, while the side chains were hold rigid in calculation with OH2 probe. Figures were prepared in PyMol v 0.99 [35], while Figure 10 is made by OE Docking Report.

Atomic charges of comp. **1** and Trp214 in excited states were obtained in MOPAC2012 [23,24], by single-point calculations with semiempirical molecular orbital PM6 method [25], using eigenvector-following optimizer and considering low dielectric constant of medium (4, characteristic for protein interior). MOPAC keywords OPEN(2,2), SINGLET, ROOT=2 (MECI calculations) have been used. The -NH- and -C(O)- termini of Trp214 were capped with Me groups. Exact coordinates of comp. **1** and Trp214, obtained from docking calculations and posterior MD minimization, as described above, were retained.

3. Results and Discussion

Intrinsic fluorescence of HSA originates from Trp214 residue, the only Trp residue in HSA. Addition of compound **1** to HSA in solution induces changes in HSA fluorescence emission spectrum (Figure 3). As it can be seen on Figure 3, fluorescence intensity decreases during the titration as the concentration of comp. **1** increases, and a slight blue shift of the HSA maximum emission wavelength (λ_{max} = 340 nm) is visible. This shows that the intrinsic fluorescence of HSA is quenched by comp. **1**. The change in the maximum emission wavelength indicates that the microenvironment around Trp214 is altered as comp. **1**/HSA complex is formed.

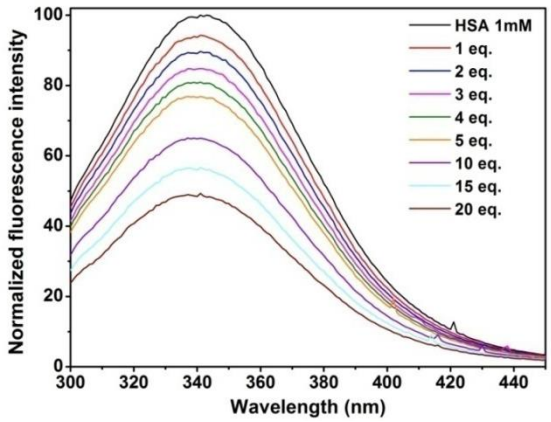

Figure 3. *Changes in HSA fluorescence emission spectra* ($c_{HSA} = 1 \times 10^{-6}$ M) *upon comp.* ***1*** *addition (*1-20 *mol equivalents), concentration of all solutions was* 1×10^{-6} *M;* $t = 37 \pm 1$ °C, pH=7.34 (1× PBS).

3.1. Quenching mechanism

Static and dynamic quenching can be distinguished on the basis of different temperature and viscosity dependence, as well as by lifetime measurements. Dynamic quenching is highly dependent upon diffusion. Higher temperatures result in faster diffusion and hence larger values for bimolecular quenching constant. On the other hand, higher temperatures will typically result in a dissociation of weakly bound complexes, and therefore decrease bimolecular quenching constant in static process.

Stern-Volmer equation (2) can be used to fit experimental data:

$$\frac{F_0}{F} = 1 + K_{sv}[Q] = 1 + k_q \tau_0 [Q] \qquad (2)$$

where F_0 and F represent HSA fluorescence intensities in absence (F_0), and in presence (F) of the quencher; K_{sv} is Stern-Volmer quenching constant (if the quenching is known to be dynamic, the Stern-Volmer constant is represented by $K_{D,}$ otherwise this constant is described as K_{SV}.), k_q is the bimolecular quenching constant, τ_0 is the lifetime of the fluorophore in the absence of quencher (in this case mean fluorescence lifetime for HSA, $\tau_0 = 7.085 \pm 0.094$ ns [36]), and [Q] is the concentration of quencher. The plot $F_0/F = f([Q])$ at three temperatures is shown on Figure 4. Results of linear regression analysis are given in Table 1.

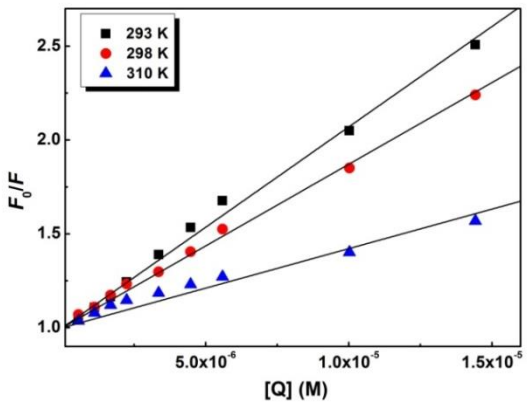

Figure 4. *Stern-Volmer plots for HSA + comp.* ***1*** *titrations at different temperatures.* $c_{HSA} = 1 \times 10^{-6}$ M, $c_{\mathbf{1}} = (0.5\text{-}13) \times 10^{-6}$ M.

Table 1. *Linear regression analysis for $F_0/F = f([Q])$ function (Equation 2) at different temperatures (Figure 4); $\tau_0 = 7.085 \pm 0.094$ ns.*

T (K)	$K_{sv} \pm$ SD (M^{-1})	$k_q \pm$ SD ($M^{-1}\ s^{-1}$)	R^2
293	$(1.07 \pm 0.02) \times 10^5$	$(1.51 \pm 0.03) \times 10^{13}$	0.999
298	$(8.7 \pm 0.1) \times 10^4$	$(1.2 \pm 0.2) \times 10^{13}$	0.999
310	$(4.2 \pm 0.2) \times 10^4$	$(5.9 \pm 0.3) \times 10^{12}$	0.999

Stern-Volmer plots (Figure 4) show good linearity, indicating single quenching type (static or dynamic). As it can be seen from Table 1, Stern-Volmer quenching constant, K_{sv}, decreases as temperature is increased, and the quenching rate constant, k_q, values are higher than the maximum scatter collision quenching constant value (2×10^{10} $M^{-1}\ s^{-1}$) [37]. All these findings confirm that the quenching mechanism in comp. **1**/HSA interaction is static.

3.2. Analysis of binding equilibria – binding constant and the number of binding sites

In order to determine preferable binding site of comp. **1** to HSA, competitive binding experiments were performed. Warfarin was used as a Sudlow site I probe, and ibuprofen as a Sudlow site II probe. HSA-site probe complexes were titrated with comp. **1** and fluorescence emission spectra recorded. Results are shown on Figure 5.

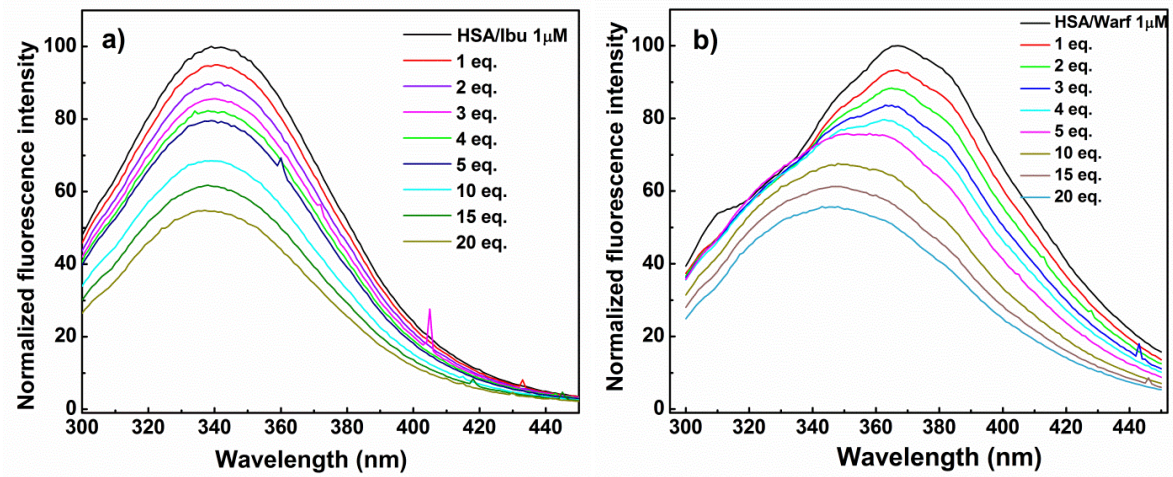

Figure 5*. Fluorescence emission spectra of:* ***a)*** *HSA-ibuprofen complex ($c_{HSA} = 1 \times 10^{-6}$ M, $c_{IBU} = 1 \times 10^{-6}$ M) and* ***b)*** *HSA-warfarin complex ($c_{HSA} = 1 \times 10^{-6}$ M, $c_{warf} = 1 \times 10^{-6}$ M) titrated with comp.* ***1*** *(1-20 mol equivalents); $t = 37 \pm 1$ °C, pH=7.34 (1× PBS).*

When small molecules bind independently to a set of equivalent sites of the protein (each binding site has the same capacity for binding of a quencher), the equilibrium between free and bound molecules for the static quenching process is given by modified Stern-Volmer equation (3):

$$\log \frac{F_0 - F}{F} = \log K_b + n \log [Q] \qquad (3)$$

where F_0 and F are corrected fluorescence intensities, in the absence and in the presence of a quencher, respectively; K_b is binding constant, and n is the number of binding sites. Linear dependence $\log(F_0\text{-}F)/F = f(\log[Q])$, shown on Figure 6, is used to obtain apparent binding constant values and the number of binding sites. Results are shown in Table 2.

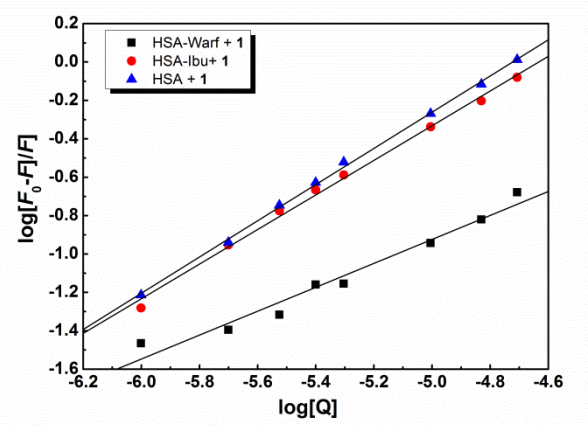

***Figure 6**. Modified Stern-Volmer plot (Equation 3) for the apparent binding constant (K_b) and the number of binding sites (n) determination in HSA/comp. **1** interaction; static quenching mechanism was assumed; t = 37±1 °C.*

***Table 2**. Apparent binding constants for comp. **1**/HSA (blank), comp. **1**/HSA-warfarin, and comp. **1**/HSA-ibuprofen interactions; t = 37±1 °C.*

	$\log K_b \pm SD$	$K_b \pm SD$ (M)	$n \pm SD$	R^2
Blank	4.45 ± 0.07	$2.8^{+0.5}_{-0.4} \times 10^4$	0.94 ± 0.01	0.999
Ibuprofen	4.2 ± 0.1	$1.5^{+0.5}_{-0.4} \times 10^4$	0.90 ± 0.02	0.995
Warfarin	2.2 ± 0.3	$1.6^{+1.2}_{-0.7} \times 10^2$	0.62 ± 0.05	0.961

Binding constant for HSA – (*R,S*)-warfarin at 37±1 °C was also experimentally determined ($\log K_b = 3.4 \pm 0.3$).

In order to check how small structural variations influence binding affinity and selectivity, mono-Me ester of comp. **1** (Figure 1) was synthesized. Comparing to comp. **1**, newly prepared compound (**2**) has only one ionisable (–COOH) group. Compounds **1** and **2** have similar molecular volumes and formally the same number of H-bond acceptors. The same set of competitive binding experiments was performed; results are shown on Figures 7 and 8, and in Table 3.

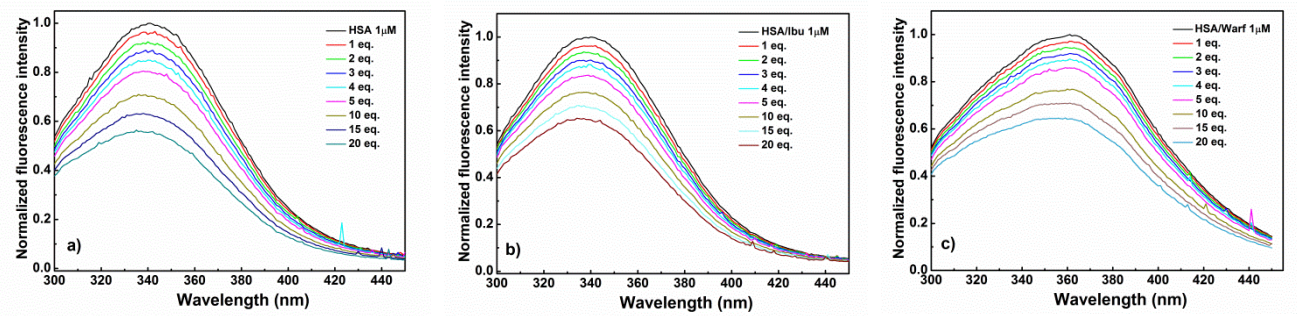

***Figure 7**. Fluorescence emission spectra of: **a)** HSA, **b)** HSA-ibuprofen complex, and **c)** HSA-warfarin complex titrated with comp. **2** (1-20 mol equivalents); concentration of all solutions was 1×10^{-6} M; t = 37±1 °C, pH=7.34 (1× PBS).*

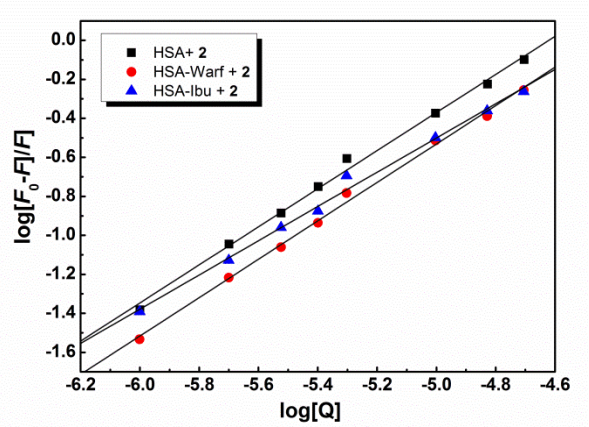

***Figure 8**. Modified Stern-Volmer plot (Equation 3) for the apparent binding constant (K_b) and the number of binding sites (n) determination in HSA-comp. **2** interaction; static quenching mechanism was assumed; t = 37 ± 1 °C.*

***Table 3.** Apparent binding constants for comp. **2**/HSA (blank), comp. **2**/HSA-warfarin, and comp. **2**/HSA-ibuprofen interactions; t = 37±1 ℃.*

	logK_b ± SD	K_b ± SD (M)	n ± SD	R^2
Blank	4.5 ± 0.1	$3.2^{+0.8}_{-0.7} \times 10^4$	0.98 ± 0.03	0.995
Ibuprofen	3.9 ± 0.2	$0.8^{+0.5}_{-0.3} \times 10^4$	0.88 ± 0.03	0.993
Warfarin	4.4 ± 0.1	$2.5^{+0.7}_{-0.5} \times 10^2$	0.99± 0.03	0.996

As it can be seen from experimental results, comp. **1** binds to warfarin binding site (Sudlow site I), while it seems that preferable site for comp. **2** binding is ibuprofen binding site (Sudlow site II). Molecular modeling studies are in agreement with experimental results.

Fluorescence data are often used to evaluate the enthalpy and entropy of complex formation. In order to study the thermodynamics of comp. **1** to HSA binding, fluorescence titration spectra were recorded and binding constant determined at several temperatures according to modified Stern-Volmer equation (3), (an example of linear fitting is shown on Figure 6). Results are shown in Table 4.

***Table 4**. Binding constant for comp. **1**/HSA interaction measured at different temperatures; log K_b values given as mean values of three times performed measurements.*

T (K)	logK_b ± SD	K_b ± SD (M)
283	4.3 ± 0.3	$2.0^{+2.0}_{-1.0} \times 10^4$
293	5.5 ± 0.2	$3.2^{+1.8}_{-1.2} \times 10^5$
298	4.9 ± 0.3	$7.9^{+7.9}_{-3.9} \times 10^4$
303	4.6 ± 0.2	$4.0^{+2.3}_{-1.5} \times 10^4$
310	4.45 ± 0.07	$3.2^{+0.8}_{-0.7} \times 10^4$
315	4.2 ± 0.3	$1.6^{+1.6}_{-0.8} \times 10^4$

As it can be seen from Table 4, determined binding constant (K_b) values have high error values, thus data fit to either linear van't Hoff equation (4):

$$\ln K_b = \frac{-\Delta H^0}{RT} + \frac{\Delta S^0}{R} \quad (4)$$

or a non-linear one (5):

$$\frac{\ln K_{d1}}{\ln K_{d2}} = \frac{\Delta H_1^0 - T_1 \Delta C_p}{R}\left(\frac{1}{T_1} - \frac{1}{T_2}\right) + \frac{\Delta C_p}{R}\ln\frac{T_2}{T_1} \quad (5)$$

where K_d stands for dissociation constants (reciprocal to K_b values), produced unreliable results. As one of the best methods to study thermodynamics of binding is isothermal titration calorimetry (ITC) [12], we plan to use this method in future experiments.

3.3. Molecular modeling

Interaction of comp. **1** with HSA was examined by molecular docking and MD. For docking and MD simulations both carboxylic groups of **1** were deprotonated to mimic the ionization state of the molecule comparable with its ionization under assay conditions. For docking, the whole structure of HSA co-crystallized with myristic acid was used. Protonation states of ionizable residues were ascribed by empirical function [38], and H atoms were added. The protein was neutralized with Na^+ counter-ions, and then embedded in sphere of explicit water molecules. System was minimized without any constraint in NAMD 2.9. In this way obtained HSA structure was used for docking.

Two out of three best docking solutions found **1** in warfarin binding site (Sudlow site I, Figure 9a); this is in agreement with experimental results. As it can be seen on Figure 9a, carboxylates of the studied compound make salt bridges with Lys195, Lys199, Arg218, and Arg257; the *tert*-Bu group makes hydrophobic interactions with Leu219, Leu238, and Ile264, but interactions of the phenyl ring, or the aroyl carbonyl group, with HSA residues were not observed. The first three docking poses found comp. **2** in Sudlow site 2 (Figure 9b). Carboxylate moiety makes polar contacts with Arg410 and Tyr411, while ester carbonyl forms H-bond with the backbone NH of the Cys392. The Me-group of the COOMe moiety makes hydrophobic contacts with Ala449. The nonpolar part of the ligand is involved in hydrophobic contacts with Val344, Leu453 and Ala449.

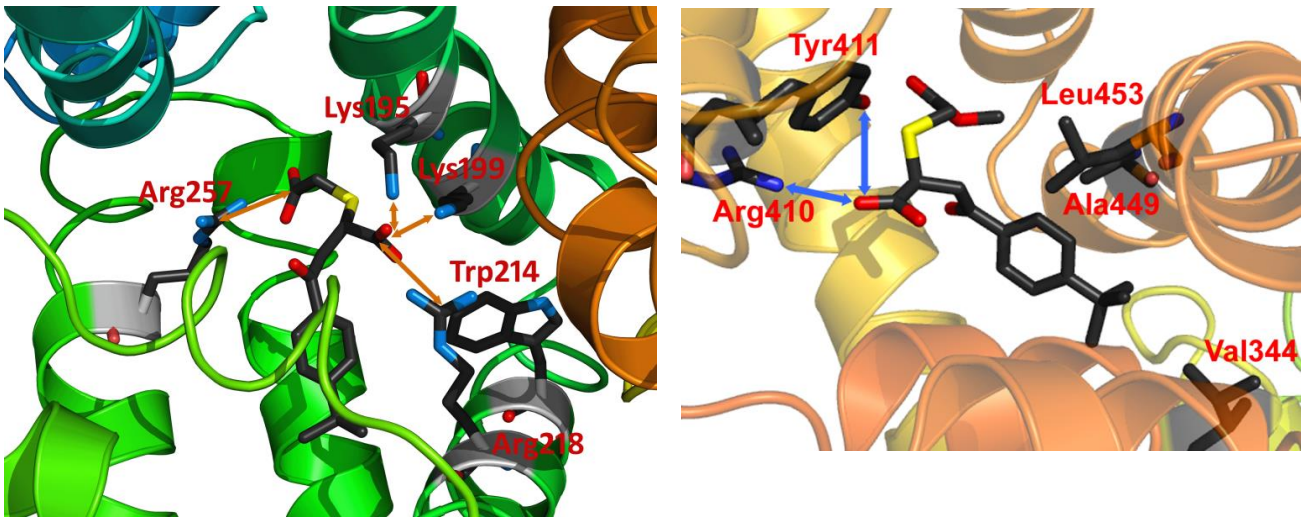

a) b)

Figure 9. *a) Comp.* ***1*** *docked to HSA. The system is depicted after energy minimization of the neutralized and solvated system. Compound is bound to Sudlow site I. Salt bridges between –COO^- groups of the studied compound and residues Lys195, Lys199, Arg218, and Arg257, observed during MD simulations, are marked by two-headed arrows. b) Comp.* ***2*** *docked to HSA. The system is depicted as obtained from the best-ranked docking solution. Polar contacts are marked by two-headed arrows.*

As AutoDock Vina provides only estimated overall energy of binding of SOM to respective biological targets, we optimized and rescored binding poses of comp. **1** and **2** by Chemgauss4 scoring function. According to results obtained, highest contribution to ligand-HSA binding should be ascribed to steric interactions. Because the cavity of Sudlow site II is more tight than the cavity of Sudlow site I, comp. **2** make more van der Waals contacts with the amino-acid residues in the Sudlow site II, comparing with the same type of contacts of the comp. **1** with the Sudlow site I (Figure 10, Table 5).

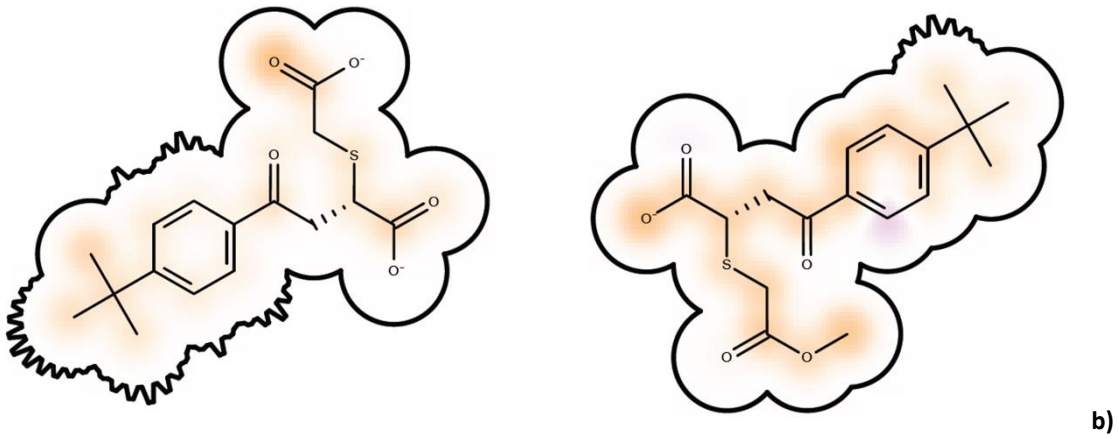

a) **b)**

Figure 10*. Schematic depiction of steric contacts between comp.* ***1*** *(a), and comp.* ***2*** *(b) with the Sudlow site I and the Sudlow site II, respectively. Solid lines represent protein contacts, notch lines – protein cavity.*

More apolar residues in Sudlow site II, comparing to Sudlow site I, causes less favorable protein desolvation term for the comp. **1** binding to Sudlow site I, comparing to the same term for the binding of comp. **2** to Sudlow site II. In this respect, it should be noted that in the frame of the Sudlow site II, global minimum (–11.4 kcal/mol) of GRID water probe was found at the very bottom of this site (Figure 13 b). This position is flanked with Ser342, Arg348, and Met446. This is in agreement with the structural features of Sudlow site II binders, bearing H-bond donors or H-bond acceptors at the termini of the hydrophobic part of molecules (naproxen, 6-MNA, iopanoic acid, etc.). As expected, ligand desolvation term is less favorable for the comp. **1** comparing to comp. **2**, as two carboxylates *vs*. one, respectively, should be desolvated. On the other hand, comp. **1** bound to the Sudlow site I makes more polar contacts (salt bridges) comparing to comp. **2** bound to Sudlow site II (polar contacts with Arg410 and Tyr411, Figure 9b), thus H-bonding term of the bound ligand is more favorable for the comp. **2**.

Table 5*. The AutoDock Vina and the Chemgauss4 scores for the best-ranked docking solutions of the comp.* ***1*** *and the comp.* ***2*** *with the HSA.*

Comp.	VINA affinity*	Total score**	Steric	Clash	ProtDesolv	LigDesolv	LigDesolvHB	HB
1	–8.4	–10.3343	–16.3915	0.3990	5.2717	4.7171	–1.2244	–3.1062
2	–7.8	–14.9374	–19.7829	0.3619	3.6944	2.8418	–0.8252	–1.2274

*In kcal/mol; **Components of score, and the total score obtained by Chemgauss scoring function are dimensionless.

As ionic bridges that tightly anchor comp. **1** to Sudlow site I were observed from docking solutions, we searched PDB database for structures of HSA cocrystallized with SOM, having similar structural features. Three such structures were found: 2BXA – CMPF (3-carboxy-4-methyl-5-propyl-2-furanpropanoic acid) bound to Sudlow site I. Carboxylates of the ligand make salt bridges with Arg222, Lys199 and Arg257 [6].

2XSI – Dansyl-L-glutamate bound to Sudlow site I. One carboxylate makes the salt bridge with Lys199, the second carboxylate is in close vicinity of Arg's 218 and 222 [39]; 2XVW – Dansyl-L-arginine bound to Sudlow site I [39]. The guanidino moiety of the ligand makes the salt bridge with the Glu153, carboxylate of the ligand is in the close vicinity of Arg218. In all three structures the two salt bridges between the ligand and side-chains of the protein are highly probable.

Afterwards, we performed molecular dynamics simulation of the comp. **1**/HSA complex, starting from the structure obtained from docking. System was set in a way similar to settings for docking. Protein with docked ligand and myristic acid molecules was neutralized, embedded in water sphere, then minimized, and heated. System prepared in this way was submitted to 3 ns of unconstrained MD simulations. Analyzing the MD trajectory, we found that examined comp. **1** is tightly bound to Sudlow site I: it was anchored by salt bridges of two carboxylates with Arg $–NH(NH_2)_2$ and Lys terminal $–NH_3$ moieties; Lys199, Lys219, Arg218, and Arg257 were involved in salt bridges.

Distances between Arg guanidino moiety and comp. **1** carboxylates were defined as $–NH\underline{C}(NH_2)_2$ to $–\underline{C}OO^-$ atoms; while distances with Lys were defined as terminal (Nξ) $–N\underline{H}_3^+$ of lysine to $–\underline{C}OO^-$ distance. Fluctuations of these distances are illustrated on Figure 11. Hydrophobic part appeared fairly more mobile, as compared to polar parts of **1**. Distances between Leu219, Leu238, Ile264, and *tert*-Bu group of **1** significantly increase (comparing to docked solution (~3.3-3.6 Å)) during first 0.5 ns of simulations; at the end of the simulation *tert*-Bu group appeared close to Leu234 and Leu260 (~3.5 Å).

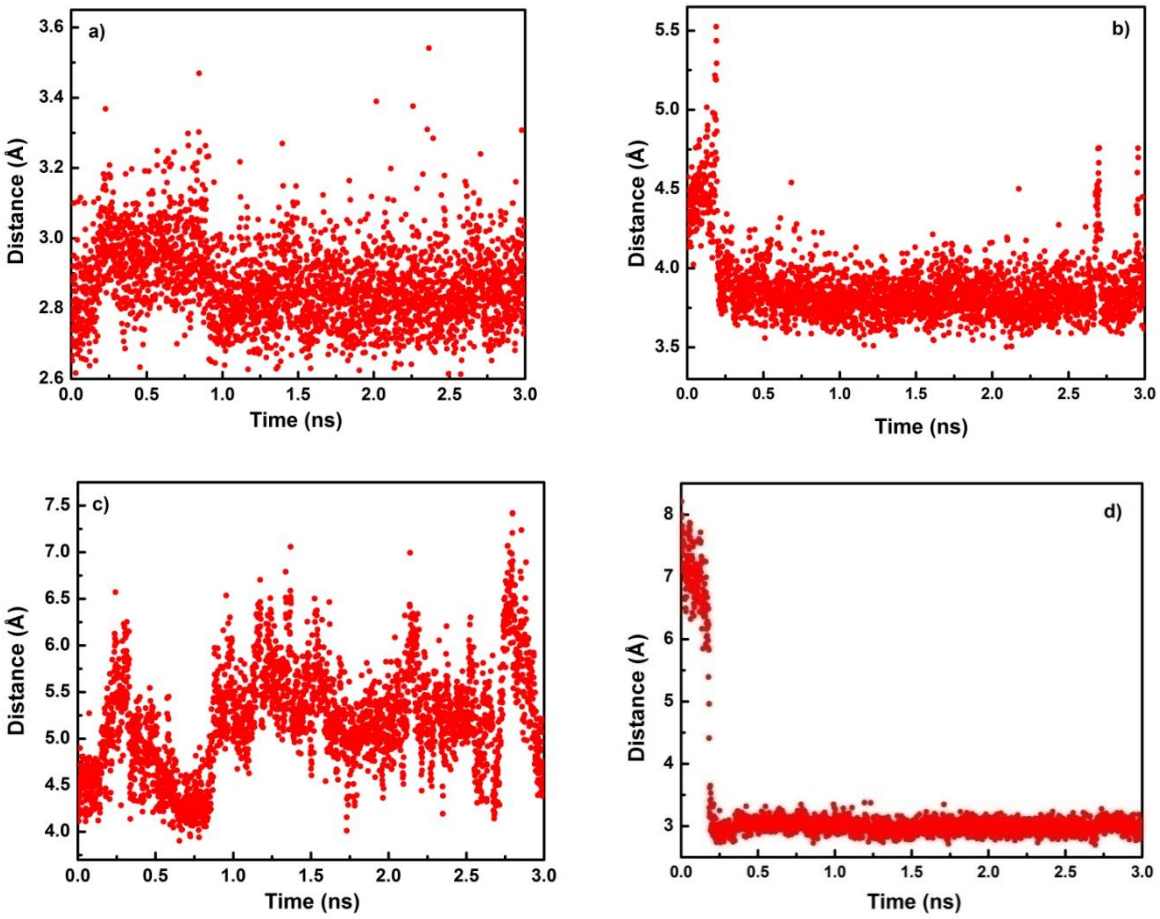

Figure 11. *Distances between:* ***a)*** *Lys199 Nξ and* comp. **1** *carboxyl C of –CH(R)-*COO^- *moiety,* ***b)*** *Arg218 C (-NH*$\underline{C}(NH_2)$ *moiety) and* comp. **1** *carboxyl C of –CH(R)-*COO^- *moiety,* ***c)*** *Arg257 C (–NH*$\underline{C}(NH_2)$ *moiety) and* comp. **1** *carboxyl C of –S-*CH_2*-*COO^- *moiety,* ***d)*** *Lys195 Nξ and* comp. **1** *carboxyl C of -CH(R)-*COO^- *moiety; all during 3 ns of MD simulations.*

Fluctuation of the 4-*tert*-Bu-Ph moiety is illustrated by the distance between centroids defined on the planes of Trp214 phenyl ring and the phenyl ring of comp. **1**, as well as by the torsion angles between those two planes (Figure 12). Trp214 is chosen because of its spatial vicinity to 4-*tert*-Bu-Ph moiety of the compound, in docking solution used for MD simulation.

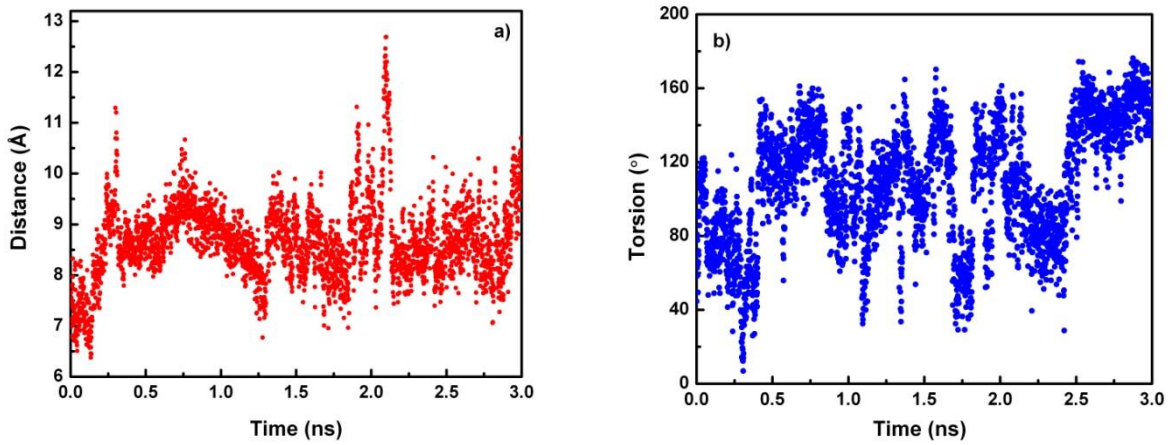

Figure 12. *a) Distance between centroids defined on Trp214 phenyl ring and the phenyl ring of comp.* ***1****, b) torsion angle between planes defined on Trp214 phenyl ring and the phenyl ring of comp.* ***1;*** *both during 3 ns of MD simulations.*

Along with docking and MD simulations, we examined HSA structure by GRID software. Interaction energies of the GRID COO^- probe (deprotonated carboxyl group) with the whole structure of HSA were calculated. Overall energy minimum (–25 kcal/mol) of the probe interaction energy was found bellow Sudlow site II (Figure 13) *i.e.* relatively far from the part of HSA where comp. **1** is bound (as concluded from experiments and modeling). Most probably, compound is too bulky to be accommodated in Sudlow site II.

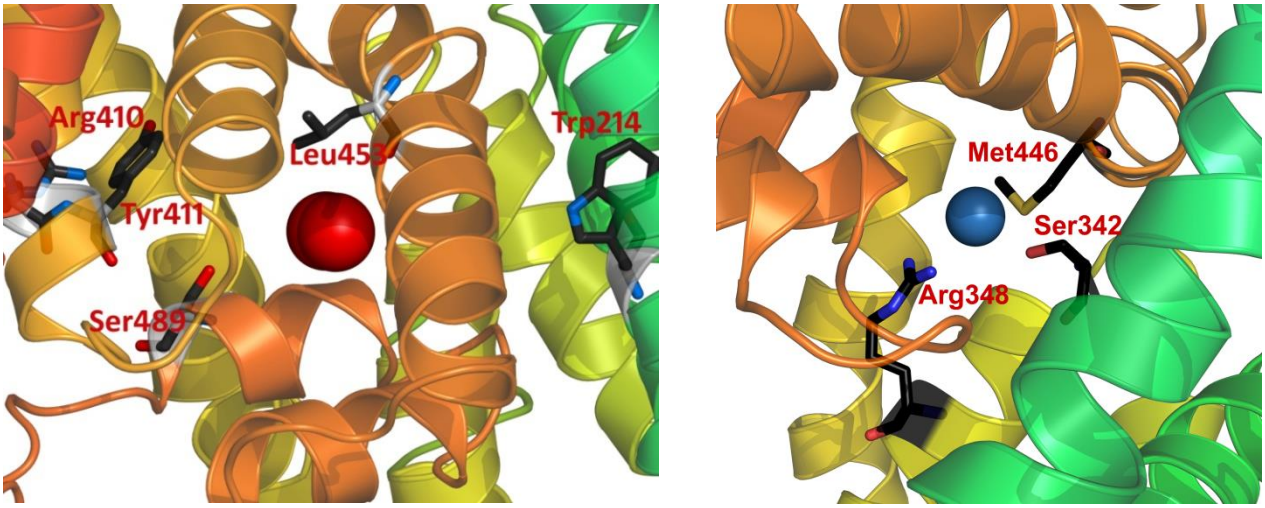

a) b)

Figure 13. *a) Position of GRID COO^- probe global minimum (–25 kcal/mol, red spheres) bellow Sudlow site II. Residues of the Sudlow site II, Arg410, Tyr411, Leu453, and Ser489, are marked. b) Position of water GRID probe global minimum (–11.4 kcal/mol, light blue sphere) in the frame of the Sudlow site II.*

3.4. Energy transfer

Fluorescence energy transfer can occur between the donor molecule in excited state (Trp214 from HSA) and the acceptor molecule in the ground state (comp. **1**). Distance between the donor and the acceptor can be calculated according to the Förster's theory of non-radiation energy transfer [40]. The energy transfer depends upon the distance between donor and acceptor, relative orientation of their dipoles, the extent to which donor emission and acceptor absorption spectra overlap, and a donor quantum yield. The energy

transfer efficiency, *E*, represents the fraction of photons absorbed by donor and transferred to the acceptor [19], and can be calculated according to the following equation (6):

$$E = 1 - \frac{F}{F_0} = \frac{R_0^6}{R_0^6 + r^6} \tag{6}$$

where *r* represents the distance between donor and acceptor; R_0 is called the Förster's distance, and represents the distance at which energy transfer is 50% efficient (it is typically in the range of 20 to 60 Å for protein-protein interactions). R_0 is calculated according to equation (7):

$$R_0^6 = 8.79 \times 10^{-25} \kappa^2 n^{-4} \phi J \tag{7}$$

where κ^2 stands for the spatial orientation factor of the dipole, *n* is a refractive index of the medium, Φ is the donor fluorescence quantum yield, and *J* is the overlap integral of the donor emission and the acceptor absorption spectra (Figure 14). The overlap integral, *J*, can be calculated according to equation (8):

$$J = \frac{\int_0^\infty F(\lambda)\varepsilon(\lambda)\lambda^4 d\lambda}{\int_0^\infty F(\lambda)d\lambda} \tag{8}$$

where $F(\lambda)$ represents normalized fluorescence intensity at wavelength λ, ε(λ) is molar absorption coefficient of the acceptor at wavelength λ. In the present study, we have used $k^2 = 2/3$ (for randomly oriented dipoles), $n = 1.336$, and $\Phi = 0.118$ [41].

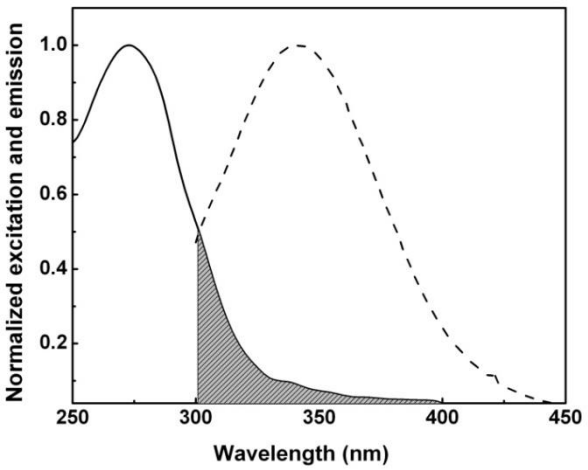

Figure 14. *Compound* ***1*** *absorption (——) and HSA (– –) emission spectra overlap*.

Using previous equations, we have calculated the overlap integral ($J = 3.26 \times 10^{-15}$ $M^{-1}cm^3$), the energy transfer efficiency ($E = 0.058$), the Förster's distance ($R_0 = 21.6$ Å), and the distance between donor (Trp214 in HSA) and acceptor (comp. **1**) ($r = 36.6$ Å). Although such results are comparable with many literature reports on the fluorescence energy transfer between HSA and ligand bound to it, obtained distance between the donor and the acceptor (36.6 Å) is inadequately high. Experimental fluorescence data showed that comp. **1** is bound to Sudlow site I. Docking study also found comp. **1** in Sudlow site I, and revealed

distance of 8.5 Å between centroids defined on aromatic moiety of Trp214 and aroyl moiety of comp. **1**. The attention was paid to κ^2 term (7), which stands for spatial orientation factor of the dipoles. κ^2 Accounts for the angle between donor and acceptor transition dipole moments, and the angle between donor/acceptor transition dipole moments and the vector joining those two dipoles. If all of these angles are 0°, $\kappa^2 = 4$; if all angles are 90°, $\kappa^2 = 0$. The κ^2 value of 2/3 is commonly used, and accounts for random distribution of the vector orientation, *i.e.* fast and complete rotation of vectors during donor excited state lifetime. For ligand bound to the protein, such assumption obviously does not hold. Movement of both Trp214 of HSA and ligand bound to HSA was constrained by the rest of the protein, and both entities could only experience rotations and the tumbling of the whole protein-ligand complex, which, for sure, did not influence spatial orientation of the dipoles. If a very small κ^2 value (0.001) is used, and all other values kept as described above, reasonable value for *r* (approx. 10 Å) is obtained. Angle between dipoles of Trp214 and comp. **1** in excited states, calculated on semiempirical level of theory, retaining spatial orientation of Trp214 and comp. **1** exactly as found by molecular docking and posterior minimization by MD, is close to 90°, as is shown on Figure 15.

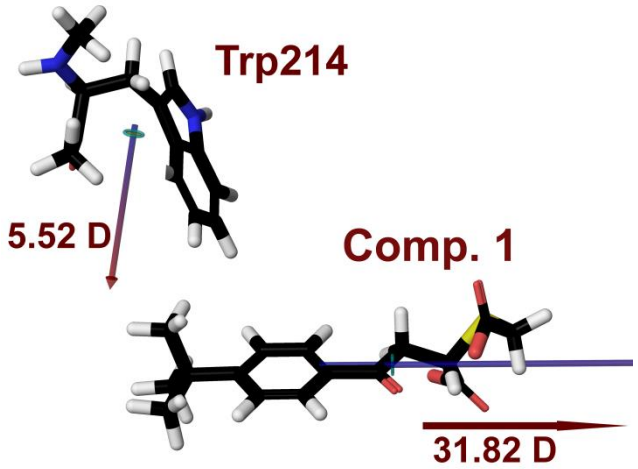

Figure 15. *Dipoles (values in Debye) of the Trp214 and the comp.* ***1*** *in excited states, calculated on semiempirical level of theory.*

4. Conclusions

Interactions between 2-[(carboxymethyl)sulfanyl]-4-oxo-4-(4-*tert*-butylphenyl)butanoic acid (comp. **1**) and its mono-Me-ester (comp. **2**) with the human serum albumin (HSA) have been studied by fluorescence spectroscopy and molecular modeling. Examined compounds have the ability to quench the intrinsic fluorescence of HSA through the static quenching mechanism. Competitive binding experiments at $t = 37 \pm 1$ °C with specific binding site probes (warfarin for Sudlow site I and ibuprofen for Sudlow site II) showed that comp. **1** selectively binds to Sudlow site I with moderate binding constant $K_b = (2.8 \pm 0.5) \times 10^4\ M^{-1}$, while comp. **2** preferably bind to Sudlow site II with binding constant $K_b = (3.2 \pm 0.9) \times 10^4\ M^{-1}$. These results, along with the estimated effective quenching constants suggest that the binding constant between comp. **1** or **2** and HSA is a moderate one. Hence, both comp. **1** and **2** can be stored and carried by HSA in the human body.

The possibility of energy resonance transfer is examined according to Förster's non-radiative energy transfer theory. According to calculated distance between HSA Trp214 and comp. **1** it was concluded that energy resonance transfer between HSA and comp. **1** is feasible process. Somewhat more detailed

consideration of terms included in calculations, reveled reasonable distance between comp. **1** and Trp214 of HSA, in accordance with other experimental data and molecular modeling.

Docking studies showed that preferable binding site of comp. **1** is Sudlow site I, while comp. **2** binds to Sudlow site II. Molecular dynamics simulations confirmed the stability of HSA complex with the comp. **1**, and the Sudlow site I as a most probable binding site.

***Acknowledgements**: Ministry of Education, Science, and Technological Development of Serbia (Grant No. 172035), the European Commission (FP7 project HP-SEE (contract number 261499) http://www.hp-see.eu/, and FP7 RegPot project FCUB ERA GA (No. 256716)) supported this work. The EC does not share responsibility for the content of the article. Authors gratefully acknowledge computational time provided by HPCG cluster, located at the Institute of Information and Communication Technologies of the Bulgarian Academy of Science (IICT-BAS). Authors gratefully acknowledge OpenEye Scientific Software, Santa Fe, NM, for the free academic licensing of software tools.*

References

[1] B.J. Drakulić, Z.D. Juranić, T.P. Stanojković, I.O. Juranić, *Journal of Medicinal Chemistry* **48** (2005) 5600-5603.

[2] B.J. Drakulić, Ž.S. Žižak, T.P. Stanojković, S. Ristić, D.M. Gođevac, I.O. Juranić, *EuroQSAR 2012 'Knowledge enabled ligand design'*, *Book of Abstracts*, Vienna, Austria, August 26-30, 2012, p. 147.

[3] T. Peters Jr. *All About Albumin, Biochemistry, Genetics, and Medical Applications*, first ed. Academic Press, San Diego, California, USA, 1995.

[4] G. Sudlow, D.J. Birkett, D.N. Wade, *Molecular Pharmacology* **11** (1975) 824-832.

[5] G. Sudlow, D.J. Birkett, D.N. Wade, *Molecular Pharmacology* **12** (1976) 1052-1061.

[6] J. Ghuman, P.A. Zunszain, I. Petitpas, A.A. Bhattacharya, M. Otagiri, S. Curry, *Journal of Molecular Biology* **353** (2005) 38-52.

[7] K. Yamasaki, V.T.G. Chuang, T. Maruyama, M. Otagiri, *Biochimica et Biophysica Acta (BBA) - General Subjects* **1830** (2013) 5435-5443.

[8] B. Meyer, T. Peters, *Angewandte Chemie International Edition* **42** (2003) 865-890.

[9] Y.S. Wang, D. Liu, D. F. Wyss, *Magnetic Resonance in Chemistry* **42** (2004) 485-489.

[10] L.V. Elst, F. Chapelle, S. Laurent, R.N. Muller, *Journal of Biological Inorganic Chemistry* **6** (2001) 196-200.

[11] L.V. Elst, F. Chapelle, S. Laurent, R.N. Muller, *Journal of Biological Inorganic Chemistry* **12** (2007) 929-937.

[12] H. Aki, M. Yamamoto, *Journal of Pharmaceutical Sciences* **83** (1994) 1712-1716.

[13] A. Sułkowska, B. Bojko, J. Równicka, W.W. Sułkowski, *Journal of Molecular Structure* **792-793** (2006) 249-256.

[14] F. Cuia, Y. Yana, Q. Zhanga, X. Yaob, G. Qua, Y. Lua, *Spectrochimica Acta Part A: Molecular and Biomolecular Spectroscopy* **74** (2009) 964-971.

[15] R. Punith, A. Hegde, S. Jaldappagari, *Journal of Fluorescence* **21** (2011) 487-495.

[16] A.C. Krüger, V. Birkedal, *Methods*, **64** (2013) 36-42.

[17] R.F. Chen, *The Journal of Biological Chemistry* **242** (1967) 173-181.

[18] M.M. Bradford, *Analytical Biochemistry* **72** (1976) 248-254.

[19] J.R. Lakowicz, *Principles of Fluorescence Spectroscopy*, third ed. Springer Science Business Media, New York, USA, 2006.

[20] P.C.D. Hawkins, A.G. Skillman, G.L. Warren, B.A. Ellingson, M.T. Stahl, *Journal of Chemical Information and Modeling* **50** (2010) 572-584.

[21] OMEGA 2.5.1.4: OpenEye Scientific Software, Santa Fe, NM. http://www.eyesopen.com.

[22] T.A. Halgren, *Journal of Computational Chemistry* **20** (1999) 720-729.

[23] J.J.P. Stewart, *Journal of Computer-Aided Molecular Design* **4** (1990) 1-105.

[24] MOPAC2012, J.J.P. Stewart, *Stewart Computational Chemistry*, Colorado Springs, CO, USA, http://OpenMOPAC.net.

[25] J.J.P. Stewart, *Journal of Molecular Modeling* **13** (2007) 1173-1213.

[26] A. Pedretti, L. Villa, G. Vistoli, *Journal of Computer-Aided Molecular Design* **18** (2004) 167-173; VegaZZ 3.0.1; http://www.ddl.unimi.it.

[27] O. Trott, A.J. Olson, *Journal of Computational Chemistry* **31** (2010) 455-461; http://vina.scripps.edu/.

[28] S. Curry, H. Mandelkow, P. Brick, N. Franks, *Nature Structural Biology* **5** (1998) 827-835.

[29] M. McGann, *Journal of Chemical Information and Modeling* **51** (2011) 578-596.

[30] G.B. McGaughey, R.P. Sheridan, C.I. Bayly, J.C. Culberson, C. Kreatsolas, S. Lindsley, V. Maiorov, J.-F. Truchon, W.D. Cornell, *Journal of Chemical Information and Modeling* **47** (2007) 1504-1519.

[31] M.R. McGann, H.R. Almond, A. Nicholls, J.A. Grant, F.K. Brown, *Biopolymers* **68** (2003) 76-90; OEDocking 3.0.1: OpenEye Scientific Software, Santa Fe, NM. http://www.eyesopen.com

[32] J.C. Phillips, R. Braun, W. Wang, J. Gumbart, E. Tajkhorshid, E. Villa, C. Chipot, R.D. Skeel, L. Kale, K. Schulten, *Journal of Computational Chemistry* **26** (2005) 1781-1802; http://www.ks.uiuc.edu/Research/namd/

[33] E. Atanassov, T. Gurov, A. Karaivanova, *Automatika and Informatika* **2** (2011) 7-11.

[34] P.J. Goodford, *Journal of Medicinal Chemistry* **28** (1985) 849-857; GRID 22c, http://www.moldiscovery.com/

[35] The PyMOL Molecular Graphics System, Version 0.99, Schrödinger, LLC; http://www.pymol.org/

[36] M. Amiri, K. Jankeje, J.R. Albani, *Journal of Fluorescence* 20 (2010) 651-656.

[37] M.R. Eftink, C.A. Ghiron, *Analytical Biochemistry* **114** (1981) 199-227.

[38] M.H.M. Olsson, C.R. Søndergaard, M. Rostkowski, J.H. Jensen, *Journal of Chemical Theory and Computation* **7** (2011) 525-537.

[39] A.J. Ryan, J. Ghuman, P.A. Zunszain, C.W. Chung, S. Curry, *Journal of Structural* Biology **174** (2011) 84-91.

[40] T. Förster, *Annalen der Physik* **437** (1948) 55-75.

[41] F.L. Cui, J. Fan, J.P. Li, Z.D. Hu, *Bioorganic and Medicinal Chemistry* **12** (2004) 151-157.